Artículo de Investigación. Revista Ciencia e Ingeniería. Vol. 47, No. 3 pp. 283-292, agosto-noviembre, 2026.
ISSN 1316-7081. ISSN Elect. 2244-8780 Universidad de los Andes (ULA)

Activated carbons derived from abundant biomass sources for reversible methane (CH_4) adsorption

Carbones activados derivados de fuentes de biomasa abundantes para la adsorción reversible de metano (CH_4).

Pérez, Patricia[1]*; Prado, Jonas[2]; Vizcaya, Marietta[1]; Rondón, Jairo[3]; Rodríguez, Pedro[2]; Lugo, Claudio[2]

[1]Laboratorio de Polímeros, Departamento de Química, Facultad de Ciencias, Universidad de Los Andes, Mérida, Venezuela.
[2]Laboratorio de Cinética y Catálisis, Departamento de Química, Facultad de Ciencias, Universidad de Los Andes, Mérida, Venezuela.
[3]Biomedical & Chemical Engineering Departments, Universidad Politécnica de Puerto Rico, San Juan, PR 00918 USA.

*perezdpatricia@gmail.com

Abstract

Carbonaceous materials were synthesized from sugarcane bagasse (BAz), coconut shells (CC), and peach kernels (SD) through carbonization followed by nitric acid activation. The materials were characterized by FTIR, XRD, and SEM analyses. FTIR results revealed functional groups typical of activated carbons, while XRD patterns showed partially amorphous graphitic structures with nanometric domains (<100 nm). SEM micrographs evidenced heterogeneous surfaces with cracks and openings, mainly in the carbons derived from BAz and SD. Finally, methane (CH_4) adsorption was evaluated, showing higher performance for activated carbons compared to non-activated carbons at 40 and 60 °C. The activated carbon obtained from sugarcane bagasse (CAs/BAz) exhibited the highest CH_4 adsorption, reaching 60.31 % at 60 °C.

Keywords: *Activated carbons, greenhouse gases, methane, adsorbent.*

Resumen

Se sintetizaron materiales carbonáceos a partir de bagazo de caña de azúcar (BAz), cáscaras de coco (CC) y semillas de durazno (SD) mediante carbonización y activación con ácido nítrico. Los materiales fueron caracterizados por FTIR, DRX y MEB. Los resultados FTIR mostraron grupos funcionales típicos de carbones activados, mientras que los patrones DRX evidenciaron estructuras grafíticas parcialmente amorfas con dominios nanométricos (<100 nm). Las micrografías MEB revelaron superficies heterogéneas con grietas y aperturas, principalmente en los carbones derivados de BAz y SD. Finalmente, se evaluó la adsorción de metano (CH_4), observándose un mayor desempeño para los carbones activados respecto a los no activados a 40 y 60 °C. El carbón activado obtenido a partir de bagazo de caña de azúcar (CAs/BAz) presentó la mayor adsorción de CH_4, alcanzando 60,31 % a 60 °C.

Palabras clave*: Carbones activados, gases de invernadero, metano, adsorbente.*

1 Introduction

Livestock production and agricultural activities have contributed significantly to the increase in anthropogenic greenhouse gas emissions, such as methane, carbon dioxide, and nitrous oxide, into the atmosphere. The increase in the concentration of these gases has contributed to global surface warming and to the deterioration of the ozone layer in the stratosphere. Among these gases, CO_2 is considered the most abundant and the main contributor to global warming.

Although the major natural and anthropogenic sources of methane worldwide (millions of tons/year) remain lower than those of CO_2, methane emissions have been increasing at a considerable rate. Furthermore, methane exhibits an environmental impact approximately 21 to 30 times greater than that of CO_2, suggesting that, over time, methane could become the predominant greenhouse gas (Carmona et al., 2005).

In this context, transportation systems operating through incomplete fuel combustion (automobiles, trucks, and motorcycles) generate waste products that are released into the environment, not only in large quantities but also with pollutants that increase the emission of gases and solid particles with severe environmental impact. Activated carbons (ACs) possess high chemical affinity, elevated porosity and surface area, and exceptional adsorption capacity. In addition, they allow adsorbate recovery and regeneration of the activated carbon used as an adsorbent material for different types of gases, thereby contributing to the reduction of environmental pollutants (Johnson et al.,

1995). Interest in these carbonaceous materials is associated with several important properties, including: (1) thermal stability, (2) resistance to acid attack, (3) predominantly hydrophobic character, (4) relatively low cost, and (5) porous structure. Consequently, in recent years, there has been a substantial increase in studies related to their synthesis and potential applications in gas adsorption and separation, as well as in industrial processes in general (Lozano, 2001).

Considering the above, the aim of this research is to synthesize activated carbons from abundant biomass sources such as sugarcane bagasse, peach kernels, and coconut shells, and to characterize them by Fourier Transform Infrared Spectroscopy (FTIR), X-ray Diffraction (XRD), and Scanning Electron Microscopy (SEM). Subsequently, their gas adsorption capacity, particularly for methane (CH_4), will be evaluated using gas chromatography, contributing to studies focused on reducing greenhouse gas emissions and, consequently, improving current climate conditions.

2 Experimental Procedure

2.1 Synthesis of Activated Carbons

Activated carbons (ACs) were synthesized from: (1) sugarcane bagasse, (2) peach kernels, and (3) coconut shells, using the modified impregnation method described by Kim and Ahn (2010) and later investigated at the Kinetics and Catalysis Laboratory of the Universidad de Los Andes by Marín† (Marín, 2015) and Prado (Prado, 2018). The synthesis procedure consisted of two main stages: the preparation of carbonaceous materials and the subsequent activation of the carbons.

2.1.1 Preparation of Carbonaceous Materials

The raw materials were treated through a carbonization process, including sugarcane bagasse (Blanco et al., 1999), peach kernels, and coconut shells (Kim and Ahn, 2010).

2.1.1.1 Carbons Derived from Sugarcane Bagasse

Sugarcane bagasse samples were washed with distilled water to remove impurities. The samples were air-dried and subsequently placed in a muffle furnace at 600 °C using a heating rate of 5 °C min^{-1} for 1 hour. The resulting solid material was sieved until a particle size less than or equal to 80 mesh (250 µm) was obtained.

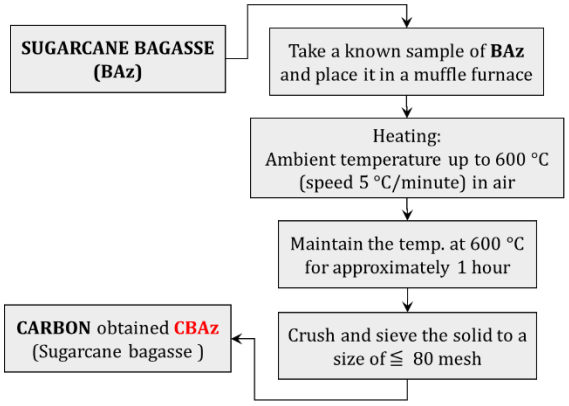

Fig. 1. Schematic representation of the preparation of carbon (CBAz) derived from sugarcane bagasse.

The carbonization process was carried out in a muffle furnace, which allowed strict control of the temperature ramp and residence time. The dried samples were heated from room temperature to 700 °C at a heating rate of 5 °C min^{-1} under an air atmosphere and maintained at this temperature for approximately 1 hour. The resulting solid was crushed, ground, and sieved until a particle size less than or equal to 80 mesh (250 µm) was obtained (Blanco et al., 1999). The schematic procedure for obtaining carbon from sugarcane bagasse is shown in Figure 1.

2.1.1.2 Carbons Derived from Peach Kernels

The collected peach kernel samples were washed with distilled water to remove residual pulp. Subsequently, the samples were placed in a drying oven at 100 °C for 5 hours. The peach kernels were then dried at 200 °C for 12 hours prior to the subsequent thermal treatment.

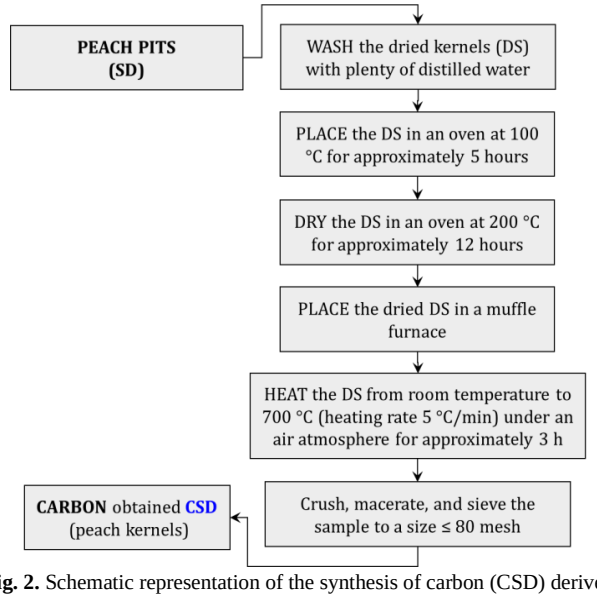

Fig. 2. Schematic representation of the synthesis of carbon (CSD) derived from peach kernels.

The carbonization process was carried out in a muffle furnace. The dried samples (~6.0 ± 0.1 kg) were heated from room temperature to 700 °C at a heating rate of 5 °C min^{-1} under an air atmosphere and maintained at 700 °C for approximately 3 hours. The resulting solid was crushed, ground, and sieved until a particle size less than or equal to 80 mesh (250 µm) was obtained (Kim and Ahn, 2010). The schematic procedure for obtaining carbon from peach kernels is shown in Figure 2.

2.1.1.3 Carbons Derived from Coconut Shells

The coconut shell samples were sanded, washed, and boiled in distilled water at approximately 100 °C for 5 hours to remove residual organic matter. Subsequently, the cleaned shells were dried in an oven at 200 °C for 12 hours prior to thermal treatment.

The carbonization process of the cleaned and dried coconut shells was carried out in a muffle furnace. The samples were heated from room temperature to 700 °C at a heating rate of 5 °C min^{-1} under an air atmosphere and maintained at 700 °C for approximately 3 hours. The resulting material was crushed, ground, and sieved to obtain a particle size close to 80 mesh (Kim and Ahn, 2010). The schematic procedure for obtaining carbon from coconut shells is shown in Figure 3.

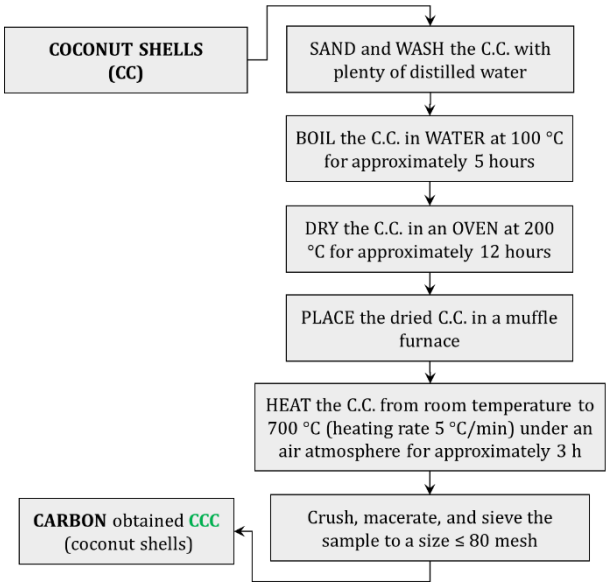

Fig. 3. Schematic representation of the synthesis of carbon (CCC) derived from coconut shells.

2.1.2 Carbon Activation

The chemical activation of the prepared carbons, obtained from sugarcane bagasse (CBAz), peach kernels (CSD), and coconut shells (CCC), was carried out in a reflux system using concentrated nitric acid (HNO_3, Merck). The first step of the activation process consisted of adding approximately 400 mL of nitric acid into a three-neck glass flask, followed by the slow addition of four (4.0) g of carbon material.

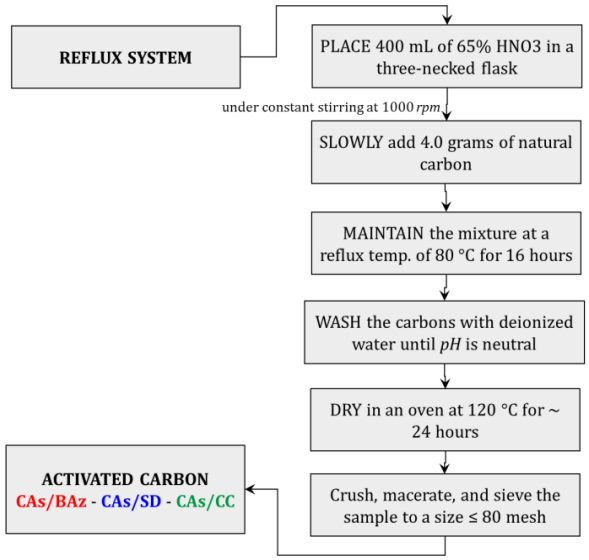

Fig. 4. Schematic representation of the activation process of the synthesized carbons (Cas/Baz, Cas/SD, and Cas/CC).

The entire process was carried out under constant stirring (~1000 rpm). Subsequently, the mixture was maintained under reflux conditions at a constant temperature of approximately 75 °C for 16 hours. After chemical activation, the resulting activated carbons were washed with abundant deionized water until neutral *pH* was reached. Finally, the activated carbons (Cas/Baz, Cas/SD, and Cas/CC) were dried in an oven at 120 °C for 24 hours (Kim and Ahn, 2010). The schematic representation of this procedure is shown in Figure 4.

2.2 Synthesized Materials

The activated carbons (Acs) obtained from different natural sources (Cas/Baz, Cas/SD, and Cas/CC) through carbonization followed by acid impregnation are presented in Table 1.

Table 1. Activated carbons obtained by carbonization/acid impregnation from different raw materials (Baz, SD, and CC).

Material	Method	Code
Carbon (Baz)	C/Ac. Imp.	CBAz
Carbon (SD)	C/Ac. Imp.	CSD
Carbon (CC)	C/Ac. Imp.	CCC
Activated carbon (Baz)	C/Ac. Imp.	Cas/Baz
Activated carbon (SD)	C/Ac. Imp.	Cas/SD
Activated carbon (CC)	C/Ac. Imp.	Cas/CC

Baz = Sugarcane bagasse; CC = Coconut shells
SD = Peach kernels; C/Ac. Imp. = Carbonization / acid impregnation

2.3 Characterization

The prepared carbonaceous materials were characterized by Fourier Transform Infrared Spectroscopy (FTIR) using a PerkinElmer Frontier infrared spectrophotometer located at the Kinetics and Catalysis Laboratory, Faculty of Sciences, Universidad de Los Andes (ULA). Powder X-ray Diffraction (XRD) analyses were performed using an automated Phillips PW 1050/25 diffractometer with Cu Kα radiation (λ = 1.5416 Å) at the Crystallography Laboratory, Faculty of Sciences, ULA. Scanning Electron Microscopy (SEM) analyses were carried out using a HITACHI S-2500 scanning electron microscope (1992 model) at the Electron Microscopy Center of the Universidad de Los Andes. All analyses were performed on both activated and non-activated samples.

3. Results and Discussion

3.1 Fourier Transform Infrared Spectroscopy (FTIR)

The infrared spectra of the synthesized carbons are shown in Figure 5. The FTIR band assignments for the non-activated carbons (CBAz, CSD, and CCC) are presented in Table 2.

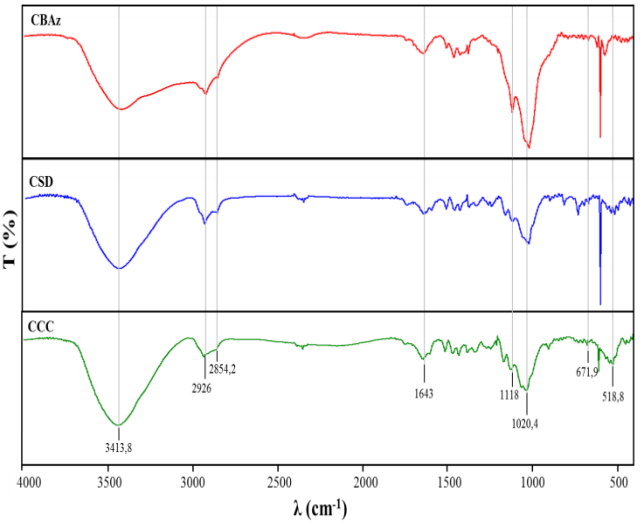

Fig. 5. FTIR spectra of non-activated carbons (CBAz, CSD, and CCC) obtained from Baz, SD, and CC.

Table 2. FTIR bands of non-activated carbons (CBAz, CSD, and CCC) obtained from Baz, SD, and CC.

ν (ref.) cm^{-1}	ν (cm^{-1})	Bond	Assignment
3400	3413.8	O–H	Symmetric and asymmetric stretching vibrations of the O–H group
2950–2845	2926–2854.2	C–H	Symmetric and asymmetric vibrations of aliphatic C–H bonds (-CH_2 -CH_3)
1650–1600	1643	C=C	Stretching vibrations of the C=C bond (aromatic compounds)
1440–880	1118–1020.4	C–H	In-plane bending vibrations of the C–H bond
650	~671.9	H–C=C	Out-of-plane bending vibrations of aromatic compounds
455	~518.8	H–C=C	Out-of-plane bending vibrations of aromatic compounds

Table 3. FTIR bands of activated carbons (Cas/Baz, Cas/SD, and Cas/CC) obtained from CBAz, CSD, and CCC.

N (ref.) cm^{-1}	ν (cm^{-1})	Bond	Assignment
3400	3403.6	O–H	Symmetric and asymmetric stretching vibrations of the O–H group
2950–2845	2928–2854.9	C–H	Symmetric and asymmetric vibrations of aliphatic C–H bonds (-CH_2 -CH_3)
1765–1645	~1720	C=O	Stretching vibrations of the C=O bond (ketones, aldehydes, lactones, or carboxylic groups)
1650–1600	1603	C=C	Stretching vibrations of the C=C bond (aromatic compounds)
1260	1202.9	C–O	Stretching vibrations of the C–O bond (esters and/or phenols)
1180	1191.8	C–O	Stretching vibrations of the C–O bond (carboxylic acids)
790	791.5	C–H	Out-of-plane bending vibrations of the C–H bond
650	726.7	C–H	In-plane bending vibrations of the carbon–hydrogen (C–H) bond
455	518.8–466	H–C=C	Out-of-plane bending vibrations of aromatic compounds

The broad band observed near 3400 cm^{-1} is attributed to stretching vibrations associated with hydroxyl groups (OH^-), indicating the presence of moisture in the synthesized samples (non-activated carbons) (Primera et al., 2011). The peaks between 2926 and 2854.2 cm^{-1} correspond to the symmetric and asymmetric vibrations of aliphatic C–H bonds (–CH_2 and –CH_3) (Rosquete, n.d.). The band at 1643 cm^{-1} is associated with stretching vibrations of the C=C bond,

characteristic of aromatic compounds (Primera et al., 2011). The absorption peaks between 1118 and 1020.4 cm^{-1} are attributed to in-plane bending vibrations of the carbon–hydrogen (C–H) bond (Primera et al., 2011). Around 671.9 cm^{-1} and 518.8 cm^{-1} (slightly shifted), characteristic signals corresponding to out-of-plane bending vibrations of aromatic compounds are observed (Yin et al., 2009).

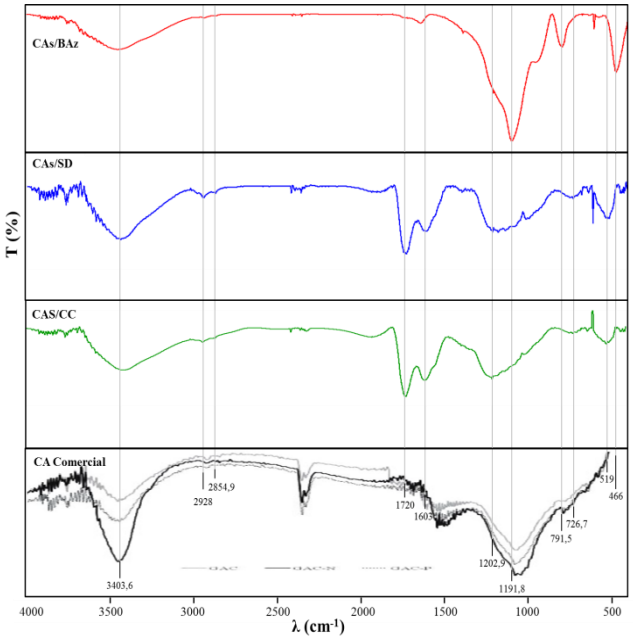

Fig. 6. FTIR spectra of activated carbons (Cas/Baz, Cas/SD, and Cas/CC) obtained from CBAz, CSD, and CCC.

The FTIR spectra of the activated carbons (Cas/Baz, Cas/SD, and Cas/CC) are presented in Figure 6 and Table 3. The broad band at approximately 3403.6 cm^{-1} corresponds to stretching vibrations of hydroxyl groups (OH^-), indicating the presence of moisture in the samples (Primera et al., 2011). The small bands between 2928 and 2854.9cm^{-1} are attributed to the symmetric and asymmetric vibrations of aliphatic C–H bonds (–CH_2 and –CH_3) (Rosquete, n.d.). The signal observed near 1720 cm^{-1} is associated with stretching vibrations of the C=O bond originating from ketones, aldehydes, lactones, or carboxylic groups (Rosquete, n.d.). The band located at 1603 cm^{-1} corresponds to stretching vibrations of the C=C bond, characteristic of aromatic compounds (Primera et al., 2011). The medium-intensity peak at 1202.9 cm^{-1} and the high-intensity peak at 1191.8 cm^{-1} correspond to stretching vibrations of the C–O bond in esters and/or phenols and carboxylic acids, respectively (Primera et al., 2011).

The bands observed near 791.5 cm^{-1} and 726.7 cm^{-1} correspond to in-plane bending vibrations of carbon–hydrogen bonds (Rosquete, n.d.). The signals at lower wavelengths, below 550 cm^{-1}, are attributed to out-of-plane bending vibrations of aromatic compounds (Yin et al., 2009).

3.2 X-ray Diffraction (XRD)

Figure 7 shows the diffraction patterns of the non-activated carbons (CBAz, CSD, and CCC) and activated carbons (Cas/Baz, Cas/SD, and Cas/CC). The identification of the phase(s) present in the synthesized carbons was performed using: (1) the X'Pert HighScore Plus 2.1 software with the PDF2-2004 database from the ICDD, which identified the presence of a hexagonal graphitic carbon-type phase (space group: P63mc), corresponding to card 00-002-0456 (Harcourt et al., 1942); and (2) comparison with articles published in recognized scientific journals (Yin et al., 2009).

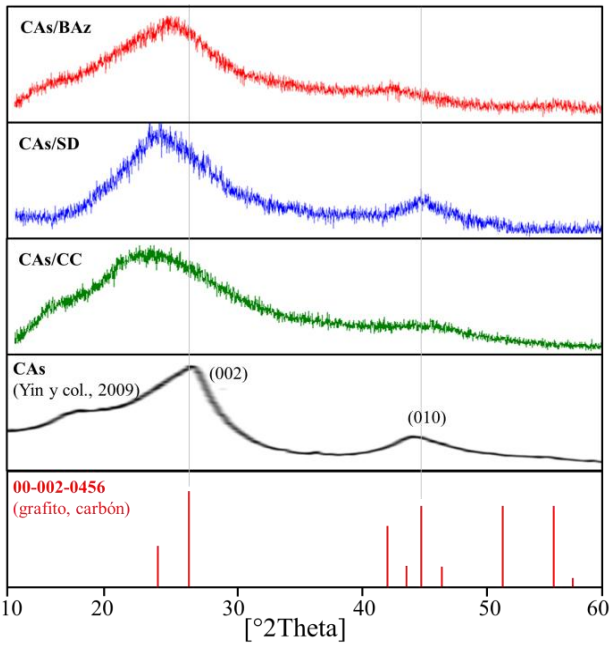

Fig. 7. XRD patterns of non-activated carbons (CBAz, CSD, and CCC) and activated carbons (Cas/Baz, Cas/SD, and Cas/CC). Activated carbon at 800 °C (Yin et al., 2009). Reference card: 00-002-0456 (Graphite).

These results indicate that the diffraction peaks obtained correspond to the (002), (010), and (111) planes, respectively. The peak associated with the (002) plane can be related to stacked-layer structures with aromatic characteristics, whereas the peaks corresponding to the (010) and (111) planes are associated with non-planar aromatic structures present in lower proportions (Yin et al., 2009).

The most intense peak observed near 25° is attributed to the formation of graphitic plates, generating a carbon–pore structure that provides experimental evidence for the presence of carbon–pore surfaces. This behavior was also reported by Rampe et al. (2011), who concluded that increasing the calcination temperature leads to a reduction in the interlayer spacing and an increase in both the crystalline diameter and the average height between the aromatic layers of the synthesized carbons. As a result, the amorphous carbon structure progressively transforms into a semicrystalline

structure with improved layer arrangement and a more stable equilibrium in the position of carbon atoms.

3.4 Scanning Electron Microscopy (SEM)

The SEM micrographs of the nitric acid-activated carbons obtained from sugarcane bagasse, peach kernels, and coconut shells are shown in Figure 8.

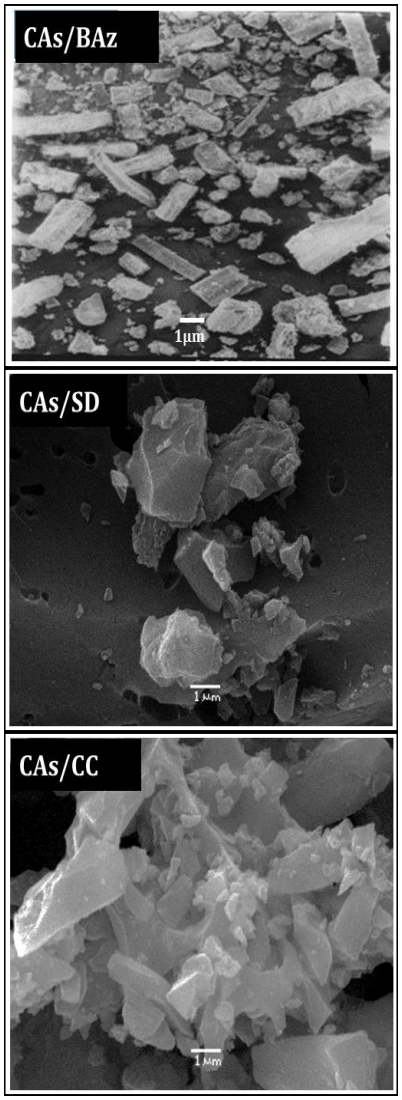

Fig. 8. Scanning Electron Microscopy (SEM) micrographs of the synthesized activated carbons: CAs/CC (coconut), CAs/SD (peach kernel), and CAs/BAz (sugarcane bagasse).

The carbons exhibited particles with sizes ranging from 1 to 10 µm, presenting highly heterogeneous morphologies. In some cases, sharp edges and generally smooth surfaces were observed, together with the presence of significant cracks and openings that influence the total surface area of the material.

CAs/CC (coconut-derived carbon) showed irregular particles with sharp edges and a highly irregular surface. However, a considerable number of dispersed particles were observed on its surface, suggesting a high specific surface area. In the case of the activated carbon CAs/SD (peach kernel-derived carbon), sharp edges and an amorphous surface were also observed, together with a significant number of cracks and openings in its morphology. The SEM micrographs of the activated carbon CAs/BAz (sugarcane bagasse-derived carbon) revealed particles of variable size with porous structure and amorphous morphology, exhibiting sharp edges and generally smooth surfaces.

Overall, the carbons obtained from coconut shells presented fewer surface irregularities compared to those derived from peach kernels and sugarcane bagasse. Nevertheless, it can be concluded that the carbonaceous adsorbents were synthesized under optimal conditions (Primera et al., 2011).

3.5 Methane (CH_4) Adsorption Test

3.5.1 Instrumental Response (Gas Chromatography)

A Hewlett-Packard gas chromatograph (HP 6890 Plus, GC System series) equipped with a thermal conductivity detector (TCD) was used for the adsorption tests. The response factor of the thermal conductivity detector was calculated using nitrogen as the carrier gas at a flow rate of 30 mL min^{-1}.

3.5.2 Pretreatment

Approximately 200 mg of non-activated carbons (CBAz, CSD, and CCC) and activated carbons (CAs/BAz, CAs/SD, and CAs/CC) were placed inside a U-shaped stainless-steel reactor. The solid pretreatment was carried out by flowing approximately 30 mL min^{-1} of nitrogen gas through the reactor while heating from room temperature to 120 °C, where the samples were maintained for 90 minutes.

3.5.3 Calibration (Gas Chromatography)

The optimization of the adsorption test conditions was achieved by calibrating parameters such as adsorbent mass, hydrocarbon flow rate, temperature range, and space velocity. The optimal conditions for studying methane adsorption on activated carbons are presented in Table 4.

Table 4. Experimental conditions for CG analyses.

Parameter	Value
Total flow rate (mL min^{-1})	~30
Temperature range (°C)	40–60
Activated carbon mass (mg)	≥ 30
Space velocity range $\times 10^{-3}$ (mL g^{-1} h^{-1})	120–240

3.5.4 System Conditions for Adsorption

After completion of the pretreatment of the carbonaceous materials, approximately 103 mL min^{-1} of a CH_4/N_2 gas mixture (3/100) was passed through the reactor according to the gas under study. The adsorbent (ACs) was subjected to a temperature ramp from room temperature to the adsorption temperatures of 40 and 60 °C, where it remained for approximately 100 minutes. The adsorption scheme is shown in Figure 9.

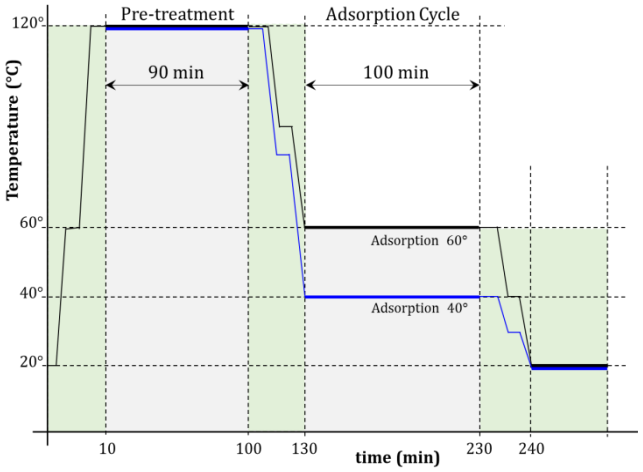

Fig. 9. Schematic representation of methane (CH_4) adsorption on non-activated carbons (CBAz, CSD, and CCC) and activated carbons (CAs/BAz, CAs/SD, and CAs/CC).

3.5.5 Adsorption Test Results

Figure 10 shows the methane (CH_4) adsorption cycle for the prepared solids, including non-activated carbons (CBAz, CSD, and CCC) and nitric acid-activated carbons (CAs/BAz, CAs/SD, and CAs/CC), within a temperature range between 40 and 60 °C. A linear methane behavior (conductimetric response measured by gas chromatography) was observed before passing through the reactor, particularly at times below 25 minutes.

Once the hydrocarbon entered the reactor containing the carbonaceous adsorbent sample, it was observed that the amount of methane adsorbed on the activated carbons increased compared to the non-activated carbons at both adsorption temperatures, 40 and 60 °C. After saturation of the adsorbent (the carbons), the initial methane concentration conditions were recovered. This increase in the adsorption capacity of the activated carbons (CAs/BAz, CAs/SD, and CAs/CC) compared to the non-activated carbons (CBAz, CSD, and CCC) may be attributed to the smaller mesopore size and lower crosslinking height of the polyaromatic molecules that constitute the carbon structure. These characteristics favor the activation process with the mineral acid, producing activated carbons with high porosity (intermediate pores) and elevated micropore volume.

These novel and interesting properties provide the activated carbons with a high adsorption capacity (Martínez et al., 2013). Furthermore, the adsorption capacity of the activated carbons increases due to surface modification, which introduces chemical species that alter the surface acidity, making it more reactive toward hydrocarbon molecules such as methane.

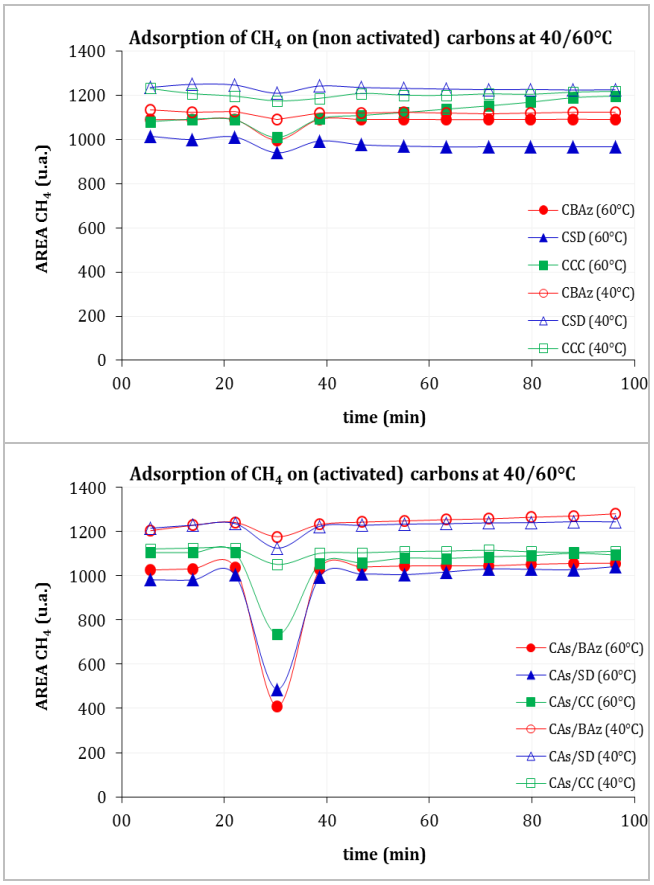

Fig. 10. Methane adsorption on non-activated carbons (CBAz, CSD, and CCC) and activated carbons (CAs/BAz, CAs/SD, and CAs/CC) at 40 and 60 °C.

The nonpolar nature of most carbon materials and the forces involved in the different adsorption processes preferentially promote the retention of nonpolar high-molecular-weight molecules (long-chain hydrocarbons, phenols, dyes, among others). In contrast, substances such as CH_4, CO_2, H_2, N_2, O_2, and even water are not readily adsorbed by carbon at room temperature. This behavior explains the experimental results obtained, where the highest methane adsorption values were observed at 60 °C, ranging from 33.5 to 60.3 % for the activated carbons (ACs), compared to the same solids tested at 40 °C, whose adsorption percentages ranged from 6.42 to 12.06 %, generally below 10.0 % (see Figure 11 and Table 5).

Table 5. Percentage methane adsorption data for non-activated carbons (CBAz, CSD, and CCC) and activated carbons (CAs/BAz, CAs/SD, and CAs/CC) at 40 and 60 °C.

Adsorbent	Time (min)	Methane Area (a.u.)	Adsorption (%)
60 °C			
CAs/BAz	30.3	409	60.32
CAs/SD	30.4	487	50.79
CAs/CC	30.4	735	33.47
CBAz	30.4	998	8.50
CSD	30.2	940	6.81
CCC	30.3	1010	7.16
40 °C			
CAs/BAz	30.4	1177	12.06
CAs/SD	30.4	1126	8.27
CAs/CC	30.4	1052	6.42
CBAz	30.4	1090	3.41
CSD	30.4	1210	2.78
CCC	30.3	1175	3.04

Figure 12 presents the methane (CH_4) adsorption capacities of the different activated carbons (CAs/BAz, CAs/SD, and CAs/CC) and non-activated carbons (CBAz, CSD, and CCC) at 40 and 60 °C. In all cases, the interaction or adsorption force between methane (adsorbate) and the carbon surface (adsorbent) is weak and mainly governed by Van der Waals interactions, favoring physisorption. Therefore, high energies are not required for hydrocarbon adsorption onto the adsorbent surface (Droguett, 1983).

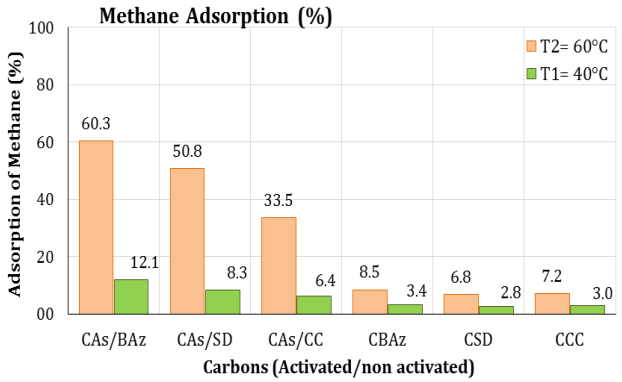

Fig. 11. Percentage methane adsorption on non-activated carbons (CBAz, CSD, and CCC) and activated carbons (CAs/BAz, CAs/SD, and CAs/CC) at 40 and 60 °C.

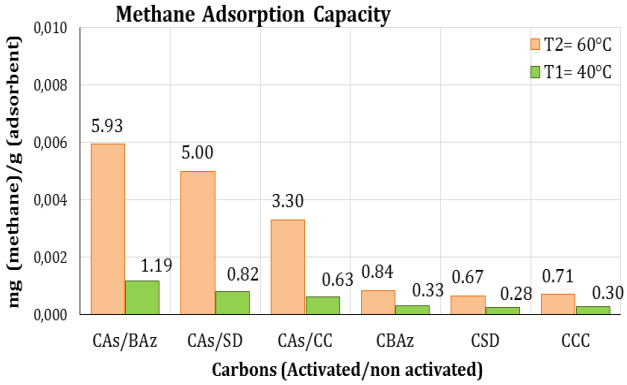

Fig. 12. Methane adsorption capacity of non-activated carbons (CBAz, CSD, and CCC) and activated carbons (CAs/BAz, CAs/SD, and CAs/CC) at 40 and 60 °C.

Table 6. Methane adsorption capacity data for non-activated carbons (CBAz, CSD, and CCC) and activated carbons (CAs/BAz, CAs/SD, and CAs/CC) at 40 and 60 °C.

Adsorbent	ppm (CH_4) adsorbed	mg (CH_4) adsorbed	Adsorption Capacity (mg g^{-1} adsorbent)	Adsorption Capacity (mg g^{-1} adsorbent)
60 °C				
CAs/BAz	9339.13	1.187	5.934	29.668
CAs/SD	7867.79	1.001	4.999	24.994
CAs/CC	5188.40	0.659	3.296	16.482
CBAz	1316.46	0.167	0.836	4.182
CSD	1053.13	0.134	0.669	3.346
CCC	1115.12	0.142	0.708	3.542
40 °C				
CAs/BAz	1874.02	0.238	1.191	5.953
CAs/SD	1285.48	0.163	0.817	4.084
CAs/CC	991.22	0.126	0.630	3.149
CBAz	526.58	0.067	0.335	1.673
CSD	433.66	0.055	0.276	1.378
CCC	464.63	0.059	0.295	1.476

g (adsorbent) = 200 mg / 1000 mg; initial CH_4 mass = 1.968 mg

The activated carbon obtained from sugarcane bagasse, CAs/BAz, tested at 60 °C (which exhibited the highest percentage adsorption among all synthesized carbons, 60.32 %), showed an adsorption capacity of approximately 1.187 mg of CH_4 per 1.968 mg of methane injected into the total 103 mL gas flow circulating through the system (Table 6).

This result indicates that the adsorption capacity of the activated carbon CAs/BAz was 5.934 mg of methane per 200 mg of initial adsorbent, corresponding to approximately 29.67 mg of methane per gram of activated carbon. A good adsorbent should exhibit an adsorption capacity between 1.5 and 20 % of its own mass, which corresponds to approximately 15-200 mg of methane adsorbed per gram of activated carbon (Hanzawa et al., 2002). The adsorption capacities of the remaining adsorbents are presented in Table 6.

4 Conclusions

The infrared spectroscopy analyses performed on the carbons before and after activation with HNO_3 revealed the presence of functional groups characteristic of carbonaceous materials, as well as nitrate groups that remained in the samples even after washing the carbonized products with deionized water.

The X-ray diffraction analyses exhibited broad diffraction peaks, indicating that the synthesized carbons possess an amorphous structure with nanometric crystalline domains (≦ 100 nm). In addition, a predominant hexagonal graphitic carbon-type phase (space group: P63mc) was identified using the PDF2-2004 ICDD database (card 00-002-0456) and through comparison with previously published scientific studies.

The SEM micrographs provided evidence of the morphology of the synthesized carbons. The particles obtained from coconut shells exhibited smaller particle sizes compared to those derived from sugarcane bagasse and peach kernels. The presence of cracks and openings in the carbon structures facilitates the penetration of gaseous molecules into the adsorbent interior, which may play a fundamental role in methane adsorption processes.

Methane adsorption tests, evaluated by gas chromatography, demonstrated that the HNO_3–activated carbons exhibited significantly higher methane adsorption capacities compared to the non-activated carbons, particularly at higher temperatures between 40 and 60 °C. After saturation of the carbon adsorbents, the initial adsorbate concentration was recovered.

Temperature had a significant influence on the adsorption process. At 60 °C, the activated carbons exhibited the highest methane adsorption capacities, with adsorption percentages ranging from 6.8 % to 60.32 %, compared to the same activated carbons tested at 40 °C, where adsorption values ranged from 2.8 % to 12.06 %.

The activated carbon obtained from sugarcane bagasse (CAs/BAz), evaluated at 60 °C, exhibited the highest methane adsorption percentage among all synthesized carbons, with approximately 1.187 mg of CH_4 adsorbed per 1.968 mg of methane injected into the 103 mL total gas flow circulating through the system.

The adsorption capacity of the activated carbon CAs/BAz was determined to be 5.934 mg of methane per 200 mg of initial adsorbent, corresponding to approximately 29.67 mg of methane per gram of activated carbon. A suitable adsorbent should exhibit an adsorption capacity between 1.5 and 20 % of its own mass, corresponding to approximately 15–200 mg of methane adsorbed per gram of activated carbon.

References

Blanco J., Bonelli P., Cerrella E., Cukierman A., (**1999**), *Activación química de bagazo de caña de azúcar para la obtención de carbones activados*. Avances en Energías Renovables y Medio Ambiente (AMERVA), Vol. 3, 1-9.

Carmona J., Bolívar D., Giraldo L., (**1989**), *El gas metano en la producción ganadera y alternativas para medir sus emisiones y aminorar su impacto a nivel ambiental y productivo*. Revista Colombiana de Ciencias Pecuarias, Vol. 18(1), 49-63.

Droguett S.E., (**1983**), *Elementos de Catálisis Heterogénea*, Serie de Química: Monografía, OEA. Programa Regional de Desarrollo Científico y Tecnológico, Número 26 de Serie de química, Universidad de Texas, USA, 43-46.

Hanzawa Y., Miyajima N., Hatori H., Yamada Y., (2002), Pore Structure and Methane Adsorption Properties of Surface Modified Activated Carbon, TANSO, Vol. 203, 123-126.

Harcourt G.A., (**1942**), Tables for the identification of ore minerals by X-ray powder patterns, *The American Mineralogist*, Vol. 27, 63-113.

Johnson K., Johnson D., (**1995**), *Methane emissions from cattle*, Department of Animal Science, Vol. 73(8), 2483-2492.

Kim K-J., Ahn H-G., (**2010**), The adsorption and desorption characteristics of a binary component system of toluene and methylethylketone on activated carbon modified with phosphoric acid, *Carbon*, Vol. 48(8), pp. 2198-2202.

Lozano D., (**2001**), Preparación y caracterización de materiales carbonosos avanzados para la separación de gases y el almacenamiento de gases y energía. [Tesis Doctoral], Departamento de Química Inorgánica, Universidad de Alicante, Alicante-España, 1-460.

Marín-Astorga† K., (**2015**), *Síntesis y caracterización de adsorbentes del tipo carbonáceos para trazas de metano*, [Trabajo Especial de Grado], Laboratorio de Cinética y Catálisis, Departamento de Química, Facultad de Ciencias, Universidad de Los Andes, Mérida-Venezuela, pp. 1-84.

Martínez M., Molina M., Rodríguez F., (**2013**), *Preparación de carbones activados con KOH a partir de residuos de petróleo*. Adsorción de hidrógeno, Departamento de química inorgánica, Universidad de Alicante, España.

Prado J., (**2018**), *Síntesis y caracterización de carbón activado obtenido a partir de residuos lignocelulósicos de la caña de azúcar, cáscara de coco y semillas de durazno y su empleo como adsorbente de CO_2, H_2 y CH_4*, [Trabajo Especial de Grado], Laboratorio de Cinética y Catálisis, Departamento de Química, Facultad de Ciencias, Universidad de Los Andes, Mérida-Venezuela, pp. 1-122.

Primera O., Colpas F., Meza E., Fernández R., (**2011**), Carbones activados a partir de bagazo de caña de azúcar y zuro de maíz para la adsorción de cadmio y plomo. *Revista de la Academia colombiana de ciencias exactas físicas y naturales*, Vol. 35(136), 387-396.

Rampe J., Setiaji B., Trisunaryanti W., Triyono I., (**2011**), Fabrication and Characterization of carbon composite from coconut shell carbon, *Indian Journal Chemistry*, Vol. 11 (2), pp.124-130.

Rosquete C., S/A. Análisis orgánico (tablas). Laboratorio de Productos Naturales, Facultad de Ciencias, Departamento de química, Universidad de los Andes.

Yin Y., Zhang J., Sheng C., (**2009**), Effect of pyrolysis temperature on the char micro-structure and reactivity of NO reduction, *Korean Journal Chemistry Engineering*, Vol. 26(3), pp. 895-901.

Received: *April 22, 2026*

Accepted: *July 7, 2026*

Pérez Dávila, Patricia: *Ph.D. in Drug Chemistry, 2017, Scientific Research Institute, Faculty of Pharmacy and Bioanalysis, Universidad de Los Andes; Professor of Polymer Laboratory at the Faculty of Sciences, ULA. Mérida, Venezuela.*

https://orcid.org/0000-0003-0591-2351

Prado Alvarado, Jonas: *Bachelor's Degree in Chemistry, 2018, Chemistry Department (Kinetics and Catalysis Laboratory) at the Faculty of Sciences, Universidad de Los Andes, Mérida. pradojonas991@gmail.com*

https://orcid.org/0009-0005-5520-2990

Vizcaya, Marietta: *Ph.D. in Drug Chemistry, 2014, Scientific Research Institute, Faculty of Pharmacy and Bioanalysis, Universidad de Los Andes; Professor of Polymer Laboratory at the Faculty of Sciences, ULA. Mérida, Venezuela. Email: marietta@ula.ve*

https://orcid.org/ 0000-0002-2064-4175

Rondón Contreras, Jairo: *Ph.D. in Applied Chemistry, mention Materials Study, 2015, Universidad de Los Andes; Professor of Biomedical & Chemical Engineering Departments, at the Polytechnic University of Puerto Rico, San Juan, PR-USA. Email: jrondon@pupr.edu*

https://orcid.org/0000-0002-9738-966X

Rodríguez Sulbarán, Pedro: *Doctor of Science in Chemistry, 2025, Universidad de Concepción, Chile; Ph.D. in Applied Chemistry, mention Materials Studies, 2015, Universidad de Los Andes; Professor of Chemistry Department (Kinetics and Catalysis Laboratory), at the Faculty of Sciences, ULA. Mérida, Venezuela. Correo electrónico: pedrojrs@gmail.com*

https://orcid.org/0000-0002-1309-8532

Lugo González, Claudio Antonio: *Ph.D. in Applied Chemistry, mention Materials Studies, 2017, Universidad de Los Andes; MSc. in Applied Chemistry, mention Materials Studies, 2009, Universidad de Los Andes; Professor of Chemistry Department (Kinetics and Catalysis Laboratory), at the Faculty of Sciences, ULA. Mérida, Venezuela. Email: claudiolugo@ula.ve*

https://orcid.org/0000-0001-8003-0354